How to cite: *Angew. Chem. Int. Ed.* **2021**, *60*, 7418–7425
International Edition: doi.org/10.1002/anie.202015060
German Edition: doi.org/10.1002/ange.202015060

Heterogeneous Catalysis

Anodic Oxidation Enabled Cation Leaching for Promoting Surface Reconstruction in Water Oxidation

Yan Duan[+], Jun Yan Lee[+], Shibo Xi, Yuanmiao Sun, Jingjie Ge, Samuel Jun Hoong Ong, Yubo Chen, Shuo Dou, Fanxu Meng, Caozheng Diao, Adrian C. Fisher, Xin Wang, Günther G. Scherer, Alexis Grimaud, and Zhichuan J. Xu**

Abstract: *A rational design for oxygen evolution reaction (OER) catalysts is pivotal to the overall efficiency of water electrolysis. Much work has been devoted to understanding cation leaching and surface reconstruction of very active electrocatalysts, but little on intentionally promoting the surface in a controlled fashion. We now report controllable anodic leaching of Cr in $CoCr_2O_4$ by activating the pristine material at high potential, which enables the transformation of inactive spinel $CoCr_2O_4$ into a highly active catalyst. The depletion of Cr and consumption of lattice oxygen facilitate surface defects and oxygen vacancies, exposing Co species to reconstruct into active Co oxyhydroxides differ from CoOOH. A novel mechanism with the evolution of tetrahedrally coordinated surface cation into octahedral configuration via non-concerted proton-electron transfer is proposed. This work shows the importance of controlled anodic potential in modifying the surface chemistry of electrocatalysts.*

Introduction

The ever-increasing consumption of fossil fuels has raised environmental concerns to an alarming point, while not fulfilling the global demand for energy which is continuously growing. This calls for the use of clean energy carriers, among which hydrogen is foreseen as a fuel of great interest for numerous industrial and chemical applications. While so-far largely produced (> 95 %) by fossil-fuel reforming, hydrogen can be sustainably produced from water electrolysis, the efficiency of which is limited by the kinetics of the oxygen evolution reaction (OER) at the anode.[1,2] To improve the sluggish reaction kinetics of OER, hence the overall efficiency for hydrogen production, recent research focuses on the development of earth-abundant transition metal oxides/(oxy)hydroxides as electrocatalysts showing promising performances in alkaline conditions.[2–9]

A rational design of catalysts can be guided by understanding their structural/elemental properties which determine the reaction mechanism and activity. Following pioneering work performed on the dimensionally stable anode (DSA) in the 70s[10] and 80s,[11,12] from 2011 onwards, several novel activity descriptors have been developed,[2,13–20] such as electron occupancy, covalency, structure and exchange interaction for transition metal oxides which can be related to M-O binding energy. While several research works have reported the surface reconstruction for some very active materials,[21–28] it remains yet almost impossible to predict the activity of these materials based on their M-O binding energy as a consequence of the constantly evolving surface during OER.[29–31] For instance, the surface of $Ba_{0.5}Sr_{0.5}Co_{0.8}Fe_{0.2}O_{3-\delta}$ (BSCF)[22,32,33] rapidly evolves into an amorphous oxyhydroxide after few cycles under OER conditions, this process is accompanied by the leaching of soluble Ba^{2+} and Sr^{2+} ions, and the dissolution and redeposition of Co^{3+} and Fe^{3+} transition metal cations.[22] Furthermore, the Sr^{2+} substitution

[*] Y. Duan,[+] J. Y. Lee,[+] Dr. Y. Sun, Dr. J. Ge, S. J. H. Ong, Dr. Y. Chen, F. Meng, Dr. Z. J. Xu
School of Materials Science and Engineering, Nanyang Technological University, 50 Nanyang Avenue, Singapore 639798 (Singapore)
E-mail: xuzc@ntu.edu.sg
Y. Duan,[+] Dr. Z. J. Xu
Energy Research Institute @ NTU, ERI@N, Interdisciplinary Graduate School, Nanyang Technological University
50 Nanyang Avenue, Singapore 639798 (Singapore)
Dr. S. Xi, Dr. C. Diao
Institute of Chemical and Engineering Sciences
Agency for Science, Technology and Research (A*STAR)
1 Pesek Road, Singapore 627833 (Singapore)
S. J. H. Ong, F. Meng, Dr. Z. J. Xu
Singapore-HUJ Alliance for Research and Enterprise, NEW-CREATE Phase II, Campus for Research Excellence and Technological Enterprise (CREATE), 1 CREATE Way, Singapore 138602 (Singapore)
Dr. Y. Chen, Dr. A. C. Fisher, Dr. Z. J. Xu
The Cambridge Centre for Advanced Research and Education in Singapore, 1 CREATE Way, Singapore 138602 (Singapore)
Dr. S. Dou, Dr. X. Wang
School of Chemical and Biomedical Engineering, Nanyang Technological University, 62 Nanyang Drive, Singapore 637459 (Singapore)
Dr. A. C. Fisher
Department of Chemical Engineering, University of Cambridge
Cambridge, CB2 3RA (UK)
Dr. G. G. Scherer
5607 Haegglingen (Switzerland)
Dr. A. Grimaud
Chimie du Solide et de l'Energie, Collège de France
UMR 8260, 75231 Cedex 05 Paris (France)
and
Réseau sur le Stockage Electrochimique de l'Energie (RS2E), CNRS FR3459, 80039 Cedex Amiens (France)
E-mail: alexis.grimaud@college-de-france.fr
[+] These authors contributed equally to this work.
Supporting information and the ORCID identification number(s) for the author(s) of this article can be found under: https://doi.org/10.1002/anie.202015060.

in $La_{1-x}Sr_xCoO_{3-\delta}$ (LSC)[23] triggers the formation of electrophilic oxygen species O^{n-} by decreasing the Fermi level energy into oxygen bands and induces a lattice oxygen participation mechanism. Several works[34–36] have shown that such lattice oxygen involvement leads to surface instabilities for LSC at large Sr^{2+} substitution level. In other catalyst systems with soluble cations, such as $CoFe_xAl_{2-x}O_4$[24] in alkaline solutions and $SrCo_{0.9}Ir_{0.1}O_{3-\delta}$,[28] Sr_2FeIrO_6[27] and $Sr_2Fe_{0.5}Ir_{0.5}O_4$[27] in acidic solutions, the leaching of cations leads to further reconstruction of surface species, which results in outstanding OER activity.

However, efforts aiming at the design of catalysts with controllable cation leaching and surface reconstruction towards a highly active surface for OER remain limited.[37] Here, we report controllable leaching of Cr from $CoCr_2O_4$ spinel oxide to promote surface reconstruction for boosting its OER activity. By activating $CoCr_2O_4$ at high potential, Cr leaching occurs and leads to the reconstruction of Co species into oxyhydroxide. The leaching increases with the applied anodic potential and is facilitated by the activation of lattice oxygen redox which gives rise to favorable surface condition for vigorous reorganization and activity enhancement. $CoCr_2O_4$ activated at 1.7 V for 1.5 hours (Act-$CoCr_2O_4$) exhibits one magnitude higher performance than pristine $CoCr_2O_4$ (Pri-$CoCr_2O_4$), which outperforms CoOOH thin film. The surface electronic structure and surface-active sites for Act-$CoCr_2O_4$ have been probed in comparison to CoOOH and NiFeOOH-Cr. This facilitates the understandings of the role Cr leaching plays in Act-$CoCr_2O_4$. Our work demonstrates a promising way to achieve controllable electrochemical reconstruction for transition metal spinel oxides. It broadens our understandings of surface evolution of spinel oxides during OER and enlightens that tunable design of highly active OER catalysts is achievable. Furthermore, it enlightens the surface regulation and activity promotion of other catalysts with soluble cations in the structure.

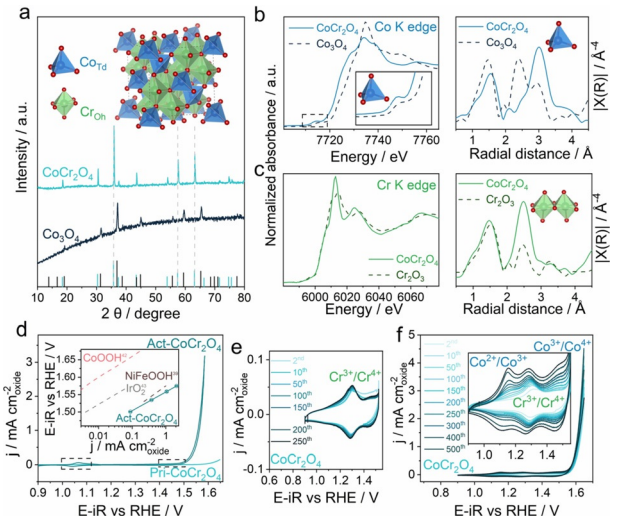

Figure 1. Crystal structure of $CoCr_2O_4$ and OER activity of Pri-$CoCr_2O_4$ and Act-$CoCr_2O_4$. a) Powder XRD patterns of the as-synthesized $CoCr_2O_4$ and Co_3O_4. The crystal structure of $CoCr_2O_4$ in spinel structure (AB_2O_4) is shown in the inset. Co_{Td} and Cr_{Oh} are tetrahedrally and octahedrally coordinated transition metal cations, respectively. b) Left: normalized Co K-edge XANES spectra for $CoCr_2O_4$. Co_3O_4 is used as a reference. Inset is the pre-edge features of Co K-edge XANES. Right: Fourier transform of the EXAFS (FT-EXAFS) for Co K-edge. The second and third peak at ca. 2.5 Å (TM_{Oh}-TM_{Oh}) and at ca. 3.0 Å (i.e. TM_{Td}-TM_{Td} or TM_{Td}-TM_{Oh}) are interatomic metal–metal distances from the absorbing metal atom Co to the second nearest-neighbor metal atoms at the octahedral or tetrahedral site. c) Normalized Cr K-edge XANES spectra (left) and FT-EXAFS for Cr K-edge (right). d) Electrochemical characterization of OER performance of $CoCr_2O_4$. CV curves of $CoCr_2O_4$ at the 2nd cycle and after Chronoamperometry (CA) at a potential of 1.7 V for 1.5 hours. Inset shows the Tafel plot for surface-area-normalized $CoCr_2O_4$ after CA at a potential of 1.7 V for 1.5 hours compared with IrO_2.[40] All data points and error bars were obtained by averaging the results of at least three independent measurements. e) CV cycling of $CoCr_2O_4$ at the low potential range prior to OER from 0.9 V to 1.52 V. f) CV cycling of $CoCr_2O_4$ in 1 M KOH at 10 mV s^{-1} from 0.9 V to 1.66 V. Inset shows the evolutive redox peaks for $CoCr_2O_4$ 2nd to 500th cycle CV in between 0.904 and 1.624 V.

Results and Discussion

The $CoCr_2O_4$ oxide was synthesized via a sol-gel method. The crystal structures of $CoCr_2O_4$ were characterized by powder X-ray diffraction (XRD). As displayed in Figure 1 a, the diffraction peaks of the as-prepared $CoCr_2O_4$ match with that of the standard cubic spinel $(Fd\bar{3}m)$ oxides. The XRD pattern of $CoCr_2O_4$ exhibits a shift to lower angles when compared to Co_3O_4. This shift is ascribed to an increase in the lattice parameter with Cr substitution. As determined by X-ray absorption near edge structure (XANES) spectroscopies, Co and Cr in $CoCr_2O_4$ possess an oxidation state of Co^{2+} and Cr^{3+}, respectively (left in Figure 1 b and Figure 1 c). A sharp Co K pre-edge (Figure 1 b left, inset) represents a transition from 1s to 3d with a strong 3d–4p orbitals mixing at non-centrosymmetric sites,[38] indicating the tetrahedral occupation[14] of Co^{2+}. This site occupation has been further confirmed with extended X-ray absorption fine structure (EXAFS). The second Fourier transform peaks reveal the distances between the absorbing metal atoms and their neighboring atoms in either the octahedral site or tetrahedral site. The distances between Co atoms and their neighboring metal cations which occupy octahedral sites are around 3.0 Å, indicating the Co atoms accommodating the center of tetrahedrons[39] (right panel in Figure 1 b). Cr atoms have 2.5 Å distance away from their neighboring metal atoms, suggesting that Cr prefers to stay in octahedral sites of $CoCr_2O_4$[39] (right in Figure 1 c).

Electrochemical measurements were then performed using the $CoCr_2O_4$ catalyst. Activities normalized by the BET surface area for the pristine material (Pri-$CoCr_2O_4$) (Table S1, Supporting Information), are presented in Figure 1 d. There, the Pri-$CoCr_2O_4$ catalyst shows limited activity in 1 M KOH. Chronoamperometry (CA) measurements were conducted on $CoCr_2O_4$ by holding the electrode at different potentials, varying from 1.5, 1.6, 1.64 to 1.7 V (all potentials are quoted in the reversible hydrogen electrode (RHE) scale), for 7 hours total. Faster stabilization for the current density at higher value is observed when applying greater potentials (Supporting Information, Figure S1). Longer time for the activation by CA at lower potential does not increase

the stabilized current density further (Supporting Information, Figure S2 and Figure S3). Besides, continuous CV cycles after CA at lower potential does not give rise to the same activity as activated at high potential. (Supporting Information, Figure S4). This potential dependent activity is presented in the Tafel plots in Supporting Information, Figure S5. It is confirmed by the decreased charge transfer resistance at higher potential as observed by electrochemical impedance spectroscopy (EIS) as shown in Supporting Information, Figure S6. After activation at a potential of 1.7 V for 1.5 hours in 1 M KOH (Act-$CoCr_2O_4$), the current becomes stable (Supporting Information, Figure S1). The current density for Act-$CoCr_2O_4$ increases more than one magnitude and becomes superior to that of IrO_2[40] (inset of Figure 1 d). By normalizing the activity by electrochemical active surface area (ECSA), (Supporting Information, Figures S7, S8, S9) the intrinsic activity for Act-$CoCr_2O_4$ exceeds that of CoOOH[41] (Supporting Information, Figure S10). This increase in activity by activation is not attributed to the chemical reaction. Indeed, after soaking the $CoCr_2O_4$ electrode in KOH for 5 hours (Supporting Information, Figure S11), the activity is not promoted at all. Besides, the possibility of the activity enhancement from the Fe contamination is excluded by using further purified KOH for the OER measurements. Details are shown in the experimental sections. As shown in the Supporting Information, Figure S12, the Tafel slopes remain at about 60 mV dec^{-1} by activating the electrode after soaking in the KOH solution for 5 hours. This confirms no Fe effect on the $CoCr_2O_4$ electrode. Instead, the effect from activation manifests in the increased electrochemical activity of cobalt surface species which as seen by the redox peaks at 1.1 V and 1.45 V characteristics of the Co^{2+}/Co^{3+} and Co^{3+}/Co^{4+} redox couples, respectively (Supporting Information Figure S13).[33,42–44] This increase in electrochemical active sites of cobalt is not observed when activating $CoCr_2O_4$ at lower potentials, that is, below 1.5 V (Supporting Information, Figure S13). Hence, cycling the pristine catalyst within a voltage range of 0.9 to 1.55 V vs. RHE, prior to OER potential, does not result in the formation of these Co redox peaks (Figure 1 e). The surface redox reaction is instead dominated by Cr species, with characteristic redox peaks from Cr^{4+}/Cr^{3+} redox couple observed at 1.3 V (Figure 1 e and Supporting Information, Figure S14). When the catalyst is subjected to a series of voltammetry cycles from 0.9 to 1.65 V, the surface redox activity is initially dominated by the redox reaction of Cr as well (Figure 1 f and Supporting Information, Figure S14). Along with cycles, two new redox peaks indicative of the activity of the Co^{2+}/Co^{3+} and Co^{3+}/Co^{4+} couples, as seen at ar. 1.1 V and 1.45 V vs. RHE, appear and gradually increase. Thus, the exposure of Co-rich electrochemical active sites to the alkaline electrolyte only occurs for $CoCr_2O_4$ after activation at a higher anodic potential. A series of CA at different potentials followed by one cycle of CV were then conducted for Pri-$CoCr_2O_4$. At a potential of around 1.56 V, there is the formation of Co redox peaks (Figure 2 a and Supporting Information, Figure S14). This is supported by the Tafel plot extracted from the CV conducted after CA (Supporting Information, Figure S5). The obviously decreased Tafel slope (after CA is held at potentials higher than 1.6 V) indicates the change in the reaction path. Besides, as the potential for CA measurement increases to 1.56 V, the current density measured at each potential starts to increase rapidly with time (Supporting Information, Figure S15). This observation differs from the one measured for Co_3O_4 which experiences a steady current density at every potential step (Supporting Information, Figure S17). Hence, while reaching a certain anodic potential (1.56 V), Co species in $CoCr_2O_4$ starts to contribute to the OER. Besides, the higher the applied anodic potential reached, the better the OER activity manifested. The largely increased electrochemical active surface area (ECSA) for Act-$CoCr_2O_4$ compared to Pri-$CoCr_2O_4$ indicates the increase in number of active sites after activation (Supporting Information, Figure S7 and Figure S8). The current density normalized by ECSA for Act-$CoCr_2O_4$ is still higher than that for Pri-$CoCr_2O_4$, indicates that not only the number of active sites but also the intrinsic activity per site increases after activation (Supporting Information, Figure S9).

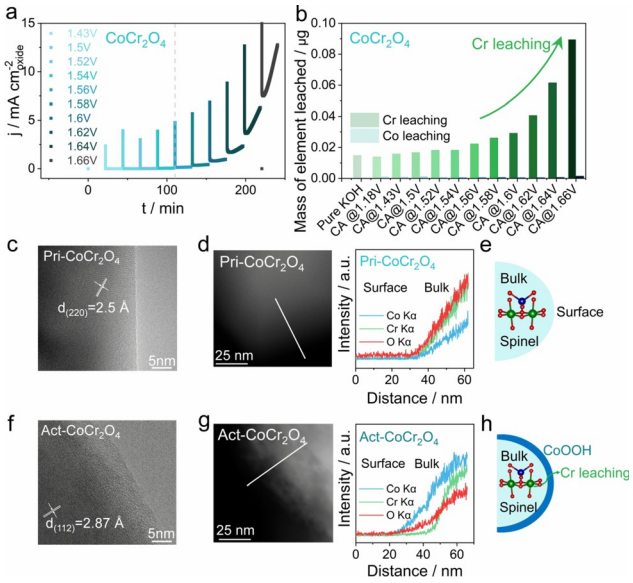

Figure 2. Analysis of surface Cr leaching and reconstruction for Act-$CoCr_2O_4$. a) A consecutive series of CA at a different potential from 1.43 to 1.66 V for $CoCr_2O_4$. b) The cumulative mass of element leached after consecutive series of CA conducted at 20mins interval for $CoCr_2O_4$. c) HRTEM image of Pri-$CoCr_2O_4$. d) STEM-EDS image and analysis for Pri-$CoCr_2O_4$. e) The bulk and surface for Pri-$CoCr_2O_4$. f) HRTEM image of Act-$CoCr_2O_4$. g) STEM-EDS image and analysis for Act-$CoCr_2O_4$. h) Schematic of Cr leaching along with the formation of oxyhydroxide on the surface for Act-$CoCr_2O_4$.

As observed by electrochemical studies, the surface redox activity for Cr cations is dominant at low potentials, while their contribution to the OER activity is minimal. Thus, Co cations dominate the surface reaction at higher potentials and contribute to the enhanced OER activity. To investigate this potentially regulated surface composition, a series of characterizations have been adopted. Inductively coupled plasma mass spectrometry (ICP-MS) was used to test the electrolytes after consecutive series of CA with an interval of 20 minutes at each potential step for $CoCr_2O_4$. In doing so, almost no

leaching of Co cations was observed in the electrolyte at the different activation potentials. However, the case is different for Cr. The cumulative mass of Cr leached is initially higher than that of Co and is accelerated after potentiostatic holding at 1.56 V vs. RHE (Figure 2b). The higher the potential at which $CoCr_2O_4$ is activated, the more Cr is leached out into the solution. Combined with the analysis of current densities under CA in Figure 2a, the occurrence and acceleration of Cr leaching synchronize with the OER activity. Hence, high-resolution transmission electron microscopy (HRTEM) reveals that the surface of Act-$CoCr_2O_4$ is forming an amorphous oxyhydroxide layer with a thickness of more than 5 nm (Figure 2c,f). To reveal the elemental composition for the surface layer of $CoCr_2O_4$ after activation, scanning transmission electron microscopy energy-dispersive X-ray spectroscopy (STEM-EDS) and line scan were conducted. The Co and Cr species are initially present in the stoichiometric proportion (1:2) on the surface of Pri-$CoCr_2O_4$, as shown in Figure 2d and Supporting Information, Figure S18. When subjected to a higher OER potential, the surface profile of Act-$CoCr_2O_4$ shows a significant depletion of Cr and the abundance of Co cations (Figure 2g; Supporting Information, Figure S19 and Figure S20). Such observation depicts well the process of Cr leaching and the gradual exposure of Co on the surface of the catalyst under increased applied potential (Figure 2e and h). This conclusion is supported by the observation via EXAFS that the local atomic structure changes for $CoCr_2O_4$ before and after the CA step. After CA at the potentials of 1.6 V and 1.64 V vs. RHE, the higher the potential at which $CoCr_2O_4$ is activated, the lower the intensity for Cr-M_{Oh} is found (Supporting Information, Figure S21), indicating more Cr leaching. Linking the observations on the change in surface elements with the electrochemical behaviors, the potential at which $CoCr_2O_4$ is activated controls the surface composition and hence the OER activity.

XANES measurements with transmission mode were then conducted before and after CA to reveal the effect of activation potential on the oxidation states and atomic structure of $CoCr_2O_4$. After CA at 1.5 V for 7 hours, the average oxidation state of Co almost does not change. The position of the Co K-edge in $CoCr_2O_4$ is found to shift towards greater energies after activation at 1.6 V or 1.64 V for 7 hours, indicating an increase in the average oxidation state of Co in $CoCr_2O_4$ (Figure 3a and Supporting Information, Figure S22). The higher the potential, the higher the oxidation state of Co is presented. The coordination environment of Co in $CoCr_2O_4$ was further investigated by extracting the Co K-edge EXAFS spectra. After CA at potentials higher than 1.6 V, the intensity for the peaks ascribed to Co-O and Co-M_{Oh} (metal cation occupied octahedral site) at around 1.5 Å and 2.5 Å increases along with potential (Figure 3b). This effect may correspond to the increase in the number of Co−O bonds[45,46] and edge shared CoO_6 octahedra. This is accompanied by a decrease in the peak intensity ascribed to Co-M_{Td} (metal cation occupied tetrahedral site) observed at around 3 Å.[14] The plausible reason for this decrease can be the formation of Co oxyhydroxide species during OER. The distance between Co atoms and their neighboring metal

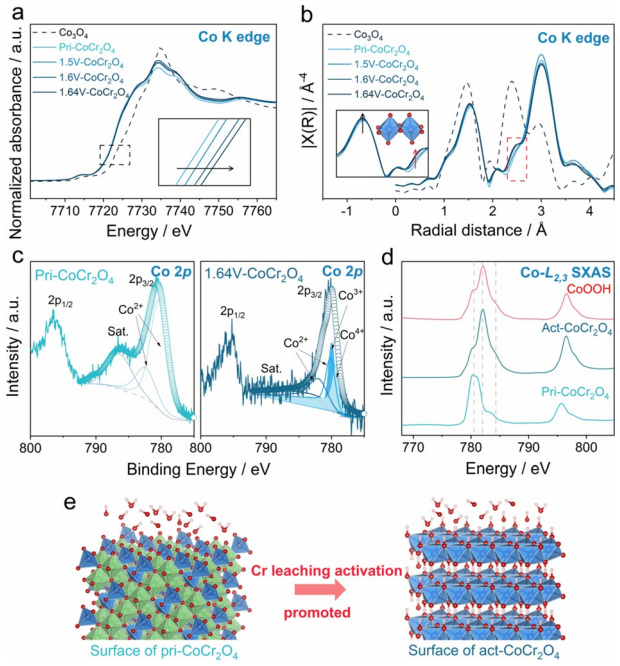

Figure 3. Evaluation of surface-active species for Act-$CoCr_2O_4$. a) Normalized Co K-edge XANES spectra for Pri-$CoCr_2O_4$ and activated $CoCr_2O_4$ after CA at a potential of 1.5/1.6/1.64 V for 7 hours. b) FT-EXAFS spectra for Co K-edge for Pri-$CoCr_2O_4$ and activated $CoCr_2O_4$ after CA at a potential of 1.5/1.6/1.64 V for 7 hours. c) XPS of Co 2p regions for the surface of Pri-$CoCr_2O_4$ (left) and $CoCr_2O_4$ activated at 1.64 V (right). Fittings of experimental spectra obtained for $CoCr_2O_4$ are shown in colored lines. d) Co L-edge soft XAS spectra for Pri-$CoCr_2O_4$ and Act-$CoCr_2O_4$ with CoOOH as reference. e) The $CoCr_2O_4$ surface before OER testing (left) and after OER activation in alkaline solution (right).

atoms are still much larger than 2.5 Å, suggesting that the surface Co is in octahedral position but the Co in the bulk remains in the tetrahedron. Indeed, as observed by HRTEM, this newly formed surface is likely amorphous without long-range order.[45,47] Altogether, these results suggest that higher applied potential is aiding the leaching of Cr, thus creating cation vacancies which result in enhanced evolution of surface Co into Co oxyhydroxide species. As analyzed by the X-ray photoelectron spectra (XPS), the Co spectra for $CoCr_2O_4$ activated at 1.6 and 1.64 V exhibit an additional peak at 781.3 eV and a satellite signal at 786.3 eV, indicative of the appearance of Co^{3+-4+} surface species on the surface after activation (Figure 3c and Supporting Information, Figure S24).[48–50] Besides, the $CoCr_2O_4$ catalyst subjected to 1.64 V vs. RHE possesses more fraction of Co^{3+-4+} on the surface compared to that activated at 1.6 V vs. RHE, which is a result of more Cr leaching and more surface Co participating in surface reconstruction. The surface Co species are also observed for Act-$CoCr_2O_4$ by a surface sensitive soft XAS technique. Co L3 and L2 peak positions in Act-$CoCr_2O_4$ spectrum shift to the position as CoOOH, which is at higher energy region compared to Pri-$CoCr_2O_4$ (Figure 3d). This suggests a higher oxidation state for Co species on the newly formed surface after activation (Figure 3e). To understand how high oxidation state for Co ions is promoted along with

Cr leaching under increasing activation potential, further characterizations on surface lattice oxygen were carried out.

The O 1s XPS spectra of $CoCr_2O_4$ samples can be deconvoluted into different contributions, with the signals at 530 eV and 531.5 eV reflecting the presence of lattice oxygen and hydroxide ions, respectively[48,51–53] (Figure 4a and Supporting Information, Figure S26). Around 50% of the surface oxygen species for the Pri-$CoCr_2O_4$ and $CoCr_2O_4$ activated at 1.5 V are composed of lattice oxygen. However, the proportion of lattice oxygen decreases to 29.5% by holding potential at 1.6 V vs. RHE and even less for that at 1.64 V vs. RHE (Figure 4b and Supporting Information, Figure S27). This shows that lattice oxygen is consumed at a high potential where Cr leaching occurs at the expense of hydroxide species deposited upon surface reconstruction (Supporting Information, Figure S27), agreeing with our TEM-EDS line scan and XAS analysis.

To understand whether the promoted surface species formation originates from the participation of lattice oxygen to the OER, as previously observed for numerous catalysts,[4,23,55,56] a gas chromatography-mass spectrometry (GC-MS) has been conducted after OER for ^{18}O labelled Pri-$CoCr_2O_4$ and Act-$CoCr_2O_4$ (Supporting Information, Figure S28 and Figure S29). Doing so, it is found that both ^{18}O labelled Pri-$CoCr_2O_4$ and Act-$CoCr_2O_4$ after OER in K^{16}OH do not release $^{18}O_2$ or $^{16}O^{18}O$ during OER (Supporting Information, Figure S30 and Figure 4c). This observation shows that the oxygen evolved is not from the lattice oxygen in $CoCr_2O_4$ either with activation or without activation. By detecting the evaporated liquid solution after OER in K^{16}OH for ^{18}O labeled Act-$CoCr_2O_4$, ^{18}OH and $H_2{}^{18}O$ are observed besides ^{16}OH and $H_2{}^{16}O$ (Figure 4d). This implies that lattice oxygen in Act-$CoCr_2O_4$ dissolves into the KOH solution after OER. This loss of lattice oxygen may originate from the leaching of soluble Cr^{6+} species.[57,58] Hence, by using ion chromatography (IC), a representative peak for Cr^{6+} ion[59] has been observed in the KOH solution after OER of Act-$CoCr_2O_4$ (Supporting Information, Figure S31). This indicates that chromate $(CrO_4)^{2-}$ are released during oxidation of Cr^{4+} species at OER potentials, that phenomenon becoming greater at higher potentials. Indeed, at 1.5 V vs. RHE, the content of lattice oxygen is almost the same as that in Pri-$CoCr_2O_4$ (Supporting Information, Figure S26), while at 1.6 V vs. RHE above the OER onset potential, lattice oxygen starts to be detected in the alkaline electrolyte as the result of the formation of chromate $(CrO_4)^{2-}$ soluble species. The continuous dissolution of Cr ions thus leaves a large amount of cation vacancies and oxygen vacancies (O_{vac}), exposing the tetrahedral Co from the surface towards the bulk. This is supported by the loss of lattice oxygen on the surface outweighing the gain in OH^- ions, as shown in Figure 4b and Supporting Information, Figure S27. This difference is a result of the O_{vac} formed on the surface. As observed by O K-edge soft XAS spectra in Figure 4e, the change in O K prepeak intensity indicates the change in metal–oxygen bonding covalency or the formation of defects in the structure. A large number of O_{vac} on the surface of Act-$CoCr_2O_4$ creates favorable conditions for the formation of amorphous Co oxyhydroxide layer[22] without long-range order by absorbing the OH^- ions from the electrolyte. This gives rise to a much enhanced OER activity (Supporting Information, Figure S10), as manifested by three orders of magnitude increase in turnover frequency (TOF) for Act-$CoCr_2O_4$ (Experimental methods and Supporting Information, S30) when compared to CoOOH (Supporting Information, S31). For CoOOH, there are more electrochemically accessible sites, however, not all sites electrochemically accessible are OER active. While for Act-$CoCr_2O_4$, Cr leaching and surface modulation not only increases the number of active sites but also the intrinsic activity per active site for Co (Supporting Information, Figure S10). That behavior is also different from NiFeOOH-Cr as reported by Xu et al. When Cr leaches, only the number of active sites increases but not the intrinsic activity per site.

To further probe the effect of activation potential on the possible reaction paths for Pri-$CoCr_2O_4$ and Act-$CoCr_2O_4$, pH-dependent experiments were conducted in 0.1 M/0.3 M/1 M KOH. The OER activity measured of Pri-$CoCr_2O_4$ and $CoCr_2O_4$ activated at 1.54 V vs. RHE shows no pH dependence (Supporting Information, Figures S35 and S36). This suggests that, when the activation of $CoCr_2O_4$ is not triggered, a conventional adsorbate evolving mechanism (AEM) with four concerted proton-electron transfer on the surface metal-ion center[60] dominates (Figure 5a) and a very stable surface is formed under OER. Nevertheless, the activity for $CoCr_2O_4$ activated at 1.54 V vs. RHE, though negligible, is a bit higher than that for Pri-$CoCr_2O_4$. From the surface redox peaks

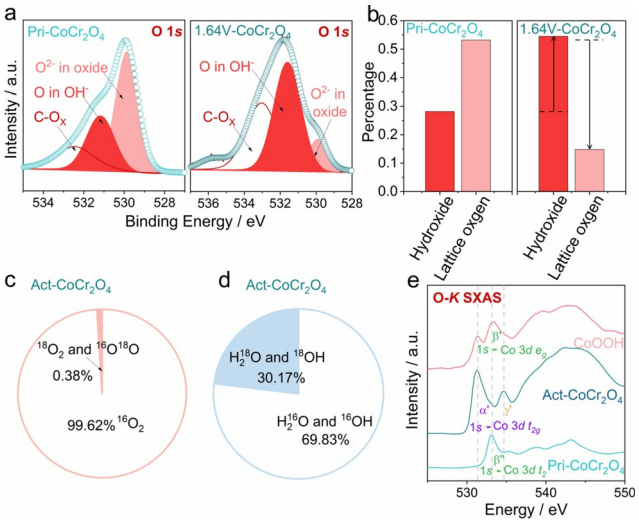

Figure 4. Probing lattice oxygen leaching for Act-$CoCr_2O_4$. a) XPS of O 1s regions for Pri-$CoCr_2O_4$ surface (left panel) and $CoCr_2O_4$ activated at 1.64 V (right panel). Fittings of experimental spectra obtained for $CoCr_2O_4$ are shown in colored lines and can be divided into three regions, which are O in C-O_x, O in OH^-, and O^{2-} in oxides.[52–54] The regions corresponding to O^{2-} in oxides are filled with light red color. b) Percentage of oxygen contained in C-O_x, OH^- and oxides for Pri-$CoCr_2O_4$ and $CoCr_2O_4$ activated at 1.64 V. c) The percentage of $^{16}O_2$ and $^{18}O_2$ & $^{16}O^{18}O$ detected by GC-MS after OER of ^{18}O labeled Act-$CoCr_2O_4$ in K^{16}OH. d) The percentage of $H_2{}^{16}O$ & ^{16}OH and $H_2{}^{18}O$ & ^{18}OH detected by GC-MS after evaporating the liquid after OER of ^{18}O labeled Act-$CoCr_2O_4$ in K^{16}OH. e) O L-edge soft XAS spectra for Pri-$CoCr_2O_4$ and Act-$CoCr_2O_4$ with CoOOH as reference.

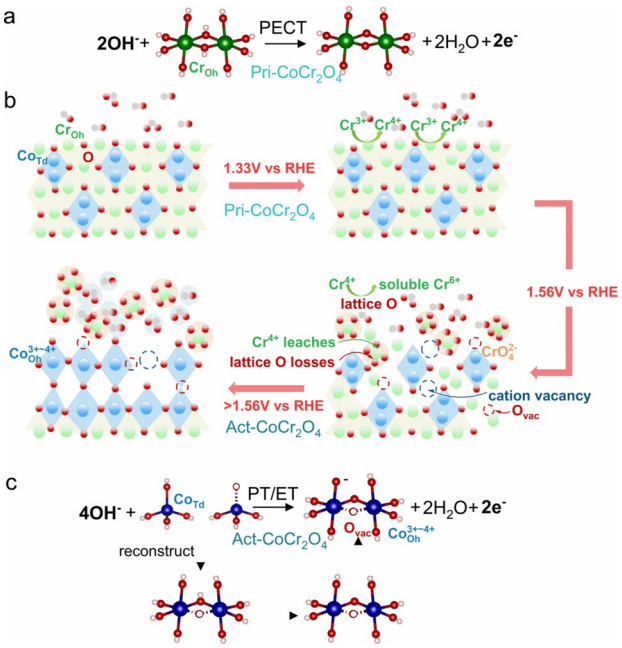

Figure 5. Activation conditions on the surface evolution mechanisms for $CoCr_2O_4$. a) Proton electron concerted transfer for Pri-$CoCr_2O_4$. b) Scheme of $CoCr_2O_4$ surface change before OER testing after being applied increased potentials. c) Proton electron non-concerted transfer for Act-$CoCr_2O_4$.

position and TEM-EDS results, the surface is found to be covered with Cr atoms. Hence, while its thickness is certainly very limited, a Cr oxyhydroxide surface layer may form after activation at a rather low potential. However, a pH-dependent OER activity is observed for $CoCr_2O_4$ activated at 1.64 V vs. RHE (Supporting Information, Figure S37), a dependence which is even greater after activation at 1.7 V vs. RHE (Supporting Information, Figure S38). This agrees with the change in Tafel slope when a potential higher than 1.6 V is applied. The pH dependence for the anodic current is often associated with lattice oxygen oxidation activity.[23] As mentioned by May et al., surface reconstruction is likely to occur via lattice oxygen participating mechanism when the O 2p center (relative to Fermi level) is higher than −2.2 eV.[32] The O 2p band center of $CoCr_2O_4$ is computed to be at −1.803 eV by DFT calculations, indicating the redox activity of lattice oxygen upon anodic polarization. However, the surface reconstruction here is very different from the one observed after the participation of lattice oxygen to the OER.[32] Here, lattice oxygen in Act-$CoCr_2O_4$ leaches concomitantly with Cr when applying a high anodic potential (> 1.56 V), leaving cation and anion vacancies on the surface. Doing so, the tetrahedrally coordinated Co cations on the surface of Pri-$CoCr_2O_4$ are isolated from each other. Since there are no adjacent metal centers bridged by oxo groups, the oxygen release following the direct coupling of dual-metal sites, as previously observed for amorphous oxyhydroxides, does not happen with cations in tetrahedral sites. Hence, $Co^{2+}{}_{Td}$ has always been considered to be an OER inactive site.[19,20] The dissolution of $Cr^{3+}{}_{Oh}$ cation stimulated at the high anodic potential in Act-$CoCr_2O_4$, fortunately, facilitates the $Co^{2+}{}_{Td}$ cations to form an octahedrally coordinated oxyhydroxide layer which does not have long-range order. This can be either $Co^{2+}{}_{Td}$ cations first lose their coordination and dissolve at the interface, then quickly re-deposit under OER conditions back onto the surface, or $Co^{2+}{}_{Td}$ cations directly form into Co oxyhydroxide (Figure 5b). The highly lacunar surface favors the absorption of hydroxides and surface Co species when compared to CoOOH film.[40] Since the surface is full of defects and oxygen vacancies are created by Cr leaching, a non-concerted proton-electron transfer[60] is demonstrated in Figure 5c and which presumably arises from the chemical exchange of hydroxyls species into the surface oxygen vacancies. The success in promoting surface reconstruction by controllable leaching of Cr in $CoCr_2O_4$ in this work makes a good example of intentional surface regulation. When the activation potential is high enough, Cr leaching is initiated. The release of lattice oxygens tremendously increases when Cr is leaching out at increasing potentials, leading to the formation of vacancies and defects and the reorganization of Co cations into oxyhydroxide. The Cr leaching not only facilitates the exposure of more surface-active sites but also increases the intrinsic activity per site, which gives rise to the promoted OER activity (Figure 5b). This intentionally controlled leaching for Act-$CoCr_2O_4$ thus enables Co in tetrahedral sites to contribute to OER by forming favorable edge-shared octahedra without long-range ordering. The only short range amorphization on the surface enables the bulk structure to be stable under more than 24 hours of stability test (Supporting Information, Figure S39).

Conclusion

We have demonstrated the promotion of surface reconstruction for $CoCr_2O_4$ via controllable leaching of Cr. This surface reconstruction by Cr leaching has been investigated by CA studies and characterization techniques such as ICP, TEM-EDS, XAS, XPS, and GC-MS. By activating $CoCr_2O_4$ at a potential higher than 1.56 V vs. RHE, the Cr leaching can be facilitated by anodic oxidation from Cr^{4+} into Cr^{6+}, triggering the leaching of lattice oxygen anions. The Cr leaching creates vacancies and defects which allows the reconstruction of Co species on the surface to form Co oxyhydroxide which possesses different electronic structures than that of CoOOH film. Higher anodic potential triggers better performance of the catalyst by promoting the Cr leaching and lattice oxygen consumption. This newly formed surface at high activation potential exhibits more Co active sites with higher intrinsic activity per sites. The OER activity for $CoCr_2O_4$ after activation at 1.7 V vs. RHE performs better than CoOOH. The catalyst is stable under 100 $mA\,cm^{-2}{}_{disk}$ for more than 24 hours. This work brings forward the design of catalyst with transition metal cations, which have different solubility as a function of oxidation state, to act as a leaching agent allowing a controlled surface activation. Controlling the activation condition is a new strategy to induce controllable metal leaching and surface reconstruction, which can enlight-

en the more rational design of electrocatalysts with the controllable reconstruction ability.

Acknowledgements

This work is supported by the Singapore MOE Tier 2 (MOE2018-T2-2-027) and the Singapore National Research Foundation under its Campus for Research Excellence and Technological Enterprise (CREATE) programme. The authors thank the Facility for Analysis, Characterization, Testing and Simulation (FACTS) in Nanyang Technological University for materials characterization.

Conflict of interest

The authors declare no conflict of interest.

Keywords: Co-based materials · controllable leaching · OER · site occupancy · surface reconstruction

[1] Y. Jiao, Y. Zheng, M. Jaroniec, S. Z. Qiao, *Chem. Soc. Rev.* **2015**, *44*, 2060 – 2086.
[2] J. Suntivich, K. J. May, H. A. Gasteiger, J. B. Goodenough, Y. Shao-Horn, *Science* **2011**, *334*, 1383 – 1385.
[3] H. Dau, C. Limberg, T. Reier, M. Risch, S. Roggan, P. Strasser, *ChemCatChem* **2010**, *2*, 724 – 761.
[4] C. Roy, B. Sebok, S. B. Scott, E. M. Fiordaliso, J. E. Sørensen, A. Bodin, D. B. Trimarco, C. D. Damsgaard, P. C. K. Vesborg, O. Hansen, I. E. L. Stephens, J. Kibsgaard, I. Chorkendorff, *Nat. Catal.* **2018**, *1*, 820 – 829.
[5] Y. Zhu, W. Zhou, Z. Shao, *Small* **2017**, *13*, 1603793.
[6] Q. Wang, K. Dastafkan, C. Zhao, *Curr. Opin. Electrochem.* **2018**, *10*, 16 – 23.
[7] Y. Pi, Q. Shao, P. Wang, F. Lv, S. Guo, J. Guo, X. Huang, *Angew. Chem. Int. Ed.* **2017**, *56*, 4502 – 4506; *Angew. Chem.* **2017**, *129*, 4573 – 4577.
[8] M. S. Burke, M. G. Kast, L. Trotochaud, A. M. Smith, S. W. Boettcher, *J. Am. Chem. Soc.* **2015**, *137*, 3638 – 3648.
[9] M. E. G. Lyons, R. L. Doyle, M. P. Browne, I. J. Godwin, A. A. S. Rovetta, *Curr. Opin. Electrochem.* **2017**, *1*, 40 – 45.
[10] A. C. C. Tseung, S. Jasem, *Electrochim. Acta Electrochim. Acta* **1977**, *22*, 31 – 34.
[11] S. Trasatti, *Electrochim. Acta* **1984**, *29*, 1503 – 1512.
[12] S. Trasatti, *J. Electroanal. Chem. Interfacial Electrochem.* **1980**, *111*, 125 – 131.
[13] W. Zhou, J. Sunarso, *J. Phys. Chem. Lett.* **2013**, *4*, 2982 – 2988.
[14] C. Wei, Z. Feng, G. G. Scherer, J. Barber, Y. Shao-Horn, Z. J. Xu, *Adv. Mater.* **2017**, *29*, 1606800.
[15] H. Li, S. Sun, S. Xi, Y. Chen, T. Wang, Y. Du, M. Sherburne, J. W. Ager, A. C. Fisher, Z. J. Xu, *Chem. Mater.* **2018**, *30*, 6839 – 6848.
[16] Y. Tong, Y. Guo, P. Chen, H. Liu, M. Zhang, L. Zhang, W. Yan, W. Chu, C. Wu, Y. Xie, *Chem* **2017**, *3*, 812 – 821.
[17] I. Yamada, A. Takamatsu, K. Asai, T. Shirakawa, H. Ohzuku, A. Seno, T. Uchimura, H. Fujii, S. Kawaguchi, K. Wada, H. Ikeno, S. Yagi, *J. Phys. Chem. C* **2018**, *122*, 27885 – 27892.
[18] R. R. Chen, Y. Sun, S. J. H. Ong, S. Xi, Y. Du, C. Liu, O. Lev, Z. J. Xu, *Adv. Mater.* **2020**, *32*, 1907976.
[19] S. Sun, Y. Sun, Y. Zhou, S. Xi, X. Ren, B. Huang, H. Liao, L. P. Wang, Y. Du, Z. J. Xu, *Angew. Chem. Int. Ed.* **2019**, *58*, 6042 – 6047; *Angew. Chem.* **2019**, *131*, 6103 – 6108.
[20] Y. Zhou, S. Sun, C. Wei, Y. Sun, P. Xi, Z. Feng, Z. J. Xu, *Adv. Mater.* **2019**, *31*, 1902509.
[21] J. S. Yoo, X. Rong, Y. Liu, A. M. Kolpak, *ACS Catal.* **2018**, *8*, 4628 – 4636.
[22] E. Fabbri, M. Nachtegaal, T. Binninger, X. Cheng, B. J. Kim, J. Durst, F. Bozza, T. Graule, R. Schäublin, L. Wiles, *Nat. Mater.* **2017**, *16*, 925.
[23] A. Grimaud, O. Diaz-Morales, B. Han, W. T. Hong, Y. L. Lee, L. Giordano, K. A. Stoerzinger, M. T. M. Koper, Y. Shao-Horn, *Nat. Chem.* **2017**, *9*, 457 – 465.
[24] T. Wu, S. Sun, J. Song, S. Xi, Y. Du, B. Chen, W. A. Sasangka, H. Liao, C. L. Gan, G. G. Scherer, L. Zeng, H. Wang, H. Li, A. Grimaud, Z. J. Xu, *Nat. Catal.* **2019**, *2*, 763 – 772.
[25] L. Trotochaud, S. W. Boettcher, *Scr. Mater.* **2014**, *74*, 25 – 32.
[26] H. Jiang, Q. He, Y. Zhang, L. Song, *Acc. Chem. Res.* **2018**, *51*, 2968 – 2977.
[27] R. Zhang, N. Dubouis, M. Ben Osman, W. Yin, M. T. Sougrati, D. A. D. Corte, D. Giaume, A. Grimaud, *Angew. Chem. Int. Ed.* **2019**, *58*, 4571 – 4575; *Angew. Chem.* **2019**, *131*, 4619 – 4623.
[28] Y. Chen, H. Li, J. Wang, Y. Du, S. Xi, Y. Sun, M. Sherburne, J. W. Ager, A. C. Fisher, Z. J. Xu, *Nat. Commun.* **2019**, *10*, 572.
[29] S. H. Chang, N. Danilovic, K. C. Chang, R. Subbaraman, A. P. Paulikas, D. D. Fong, M. J. Highland, P. M. Baldo, V. R. Stamenkovic, J. W. Freeland, *Nat. Commun.* **2014**, *5*, 4191.
[30] O. Diaz-Morales, D. Ferrus-Suspedra, M. T. M. Koper, *Chem. Sci.* **2016**, *7*, 2639 – 2645.
[31] N. Danilovic, R. Subbaraman, K. C. Chang, S. H. Chang, Y. J. Kang, J. Snyder, A. P. Paulikas, D. Strmcnik, Y. T. Kim, D. Myers, V. R. Stamenkovic, N. M. Markovic, *J. Phys. Chem. Lett.* **2014**, *5*, 2474 – 2478.
[32] K. J. May, C. E. Carlton, K. A. Stoerzinger, M. Risch, J. Suntivich, Y. L. Lee, A. Grimaud, Y. Shao-Horn, *J. Phys. Chem. Lett.* **2012**, *3*, 3264 – 3270.
[33] X. Cheng, B. J. Kim, E. Fabbri, T. J. Schmidt, *ACS Appl. Mater. Interfaces* **2019**, *11*, 34787 – 34795.
[34] W. T. Hong, K. A. Stoerzinger, Y. L. Lee, L. Giordano, A. Grimaud, A. M. Johnson, J. Hwang, E. J. Crumlin, W. Yang, Y. Shao-Horn, *Energy Environ. Sci.* **2017**, *10*, 2190 – 2200.
[35] J. T. Mefford, X. Rong, A. M. Abakumov, W. G. Hardin, S. Dai, A. M. Kolpak, K. P. Johnston, K. J. Stevenson, *Nat. Commun.* **2016**, *7*, 11053.
[36] C. Yang, C. Laberty-Robert, D. Batuk, G. Cibin, A. V. Chadwick, V. Pimenta, W. Yin, L. Zhang, J. M. Tarascon, A. Grimaud, *J. Phys. Chem. Lett.* **2017**, *8*, 3466 – 3472.
[37] Z. J. Xu, *Sci. China Mater.* **2020**, *63*, 3 – 7.
[38] D. Carta, M. F. Casula, A. Falqui, D. Loche, G. Mountjoy, C. Sangregorio, A. Corrias, *J. Phys. Chem. C* **2009**, *113*, 8606 – 8615.
[39] M. Wang, L. Árnadóttir, Z. J. Xu, Z. Feng, *Nano Micro Lett.* **2019**, *11*, 47.
[40] Y. Lee, J. Suntivich, K. J. May, E. E. Perry, Y. Shao-Horn, *J. Phys. Chem. Lett.* **2012**, *3*, 399 – 404.
[41] Y. Duan, N. Dubouis, J. Huang, D. A. D. Corte, Z. J. Xu, A. Grimaud, *ACS Catal.* **2020**, *10*, 4160 – 4170.
[42] I. Abidat, N. Bouchenafa-Saib, A. Habrioux, C. Comminges, C. Canaff, J. Rousseau, T. W. Napporn, D. Dambournet, O. Borkiewicz, K. B. Kokoh, *J. Mater. Chem. A* **2015**, *3*, 17433 – 17444.
[43] L. Wu, Q. Li, C. H. Wu, H. Zhu, A. Mendoza-Garcia, B. Shen, J. Guo, S. Sun, *J. Am. Chem. Soc.* **2015**, *137*, 7071 – 7074.
[44] Y. Yamashita, P. Barpanda, Y. Yamada, A. Yamada, *ECS Electrochem. Lett.* **2013**, *2*, A75 – A77.
[45] M. Risch, A. Grimaud, K. J. May, K. A. Stoerzinger, T. J. Chen, A. N. Mansour, Y. Shao-Horn, *J. Phys. Chem. C* **2013**, *117*, 8628 – 8635.
[46] S. Song, J. Zhou, X. Su, Y. Wang, J. Li, L. Zhang, G. Xiao, C. Guan, R. Liu, S. Chen, H. J. Lin, S. Zhang, J. Q. Wang, *Energy Environ. Sci.* **2018**, *11*, 2945 – 2953.

[47] S. H. Ye, Z. X. Shi, J. X. Feng, Y. X. Tong, G. R. Li, *Angew. Chem. Int. Ed.* **2018**, *57*, 2672 – 2676; *Angew. Chem.* **2018**, *130*, 2702 – 2706.
[48] J. Yang, H. Liu, W. N. Martens, R. L. Frost, *J. Phys. Chem. C* **2010**, *114*, 111 – 119.
[49] N. S. McIntyre, M. G. Cook, *Anal. Chem.* **1975**, *47*, 2208 – 2213.
[50] B. Liu, Y. Zhang, L. Tang, *Int. J. Hydrogen Energy* **2009**, *34*, 435 – 439.
[51] L. Liardet, X. Hu, *ACS Catal.* **2018**, *8*, 644 – 650.
[52] K. A. Stoerzinger, W. T. Hong, E. J. Crumlin, H. Bluhm, M. D. Biegalski, Y. Shao-Horn, *J. Phys. Chem. C* **2014**, *118*, 19733 – 19741.
[53] K. A. Stoerzinger, X. Renshaw Wang, J. Hwang, R. R. Rao, W. T. Hong, C. M. Rouleau, D. Lee, Y. Yu, E. J. Crumlin, Y. Shao-Horn, *Top. Catal.* **2018**, *61*, 2161 – 2174.
[54] K. A. Stoerzinger, L. Wang, H. Su, K. J. Lee, E. J. Crumlin, Y. Du, *Appl. Surf. Sci.* **2020**, *527*, 146919.
[55] S. Lee, K. Banjac, M. Lingenfelder, X. Hu, *Angew. Chem. Int. Ed.* **2019**, *58*, 10295 – 10299; *Angew. Chem.* **2019**, *131*, 10401 – 10405.
[56] Y. Surendranath, M. W. Kanan, D. G. Nocera, *J. Am. Chem. Soc.* **2010**, *132*, 16501 – 16509.
[57] T. L. Rinehart, D. G. Schulze, R. M. Bricka, S. Bajt, E. R. Blatchley, *J. Hazard. Mater.* **1997**, *52*, 213 – 221.
[58] D. Xu, M. B. Stevens, Y. Rui, G. DeLuca, S. W. Boettcher, E. Reichmanis, Y. Li, Q. Zhang, H. Wang, *Electrochim. Acta* **2018**, *265*, 10 – 18.
[59] R. Michalski, *Pol. J. Environ. Stud.* **2004**, *13*, 73 – 77.
[60] M. Görlin, J. Ferreira de Araújo, H. Schmies, D. Bernsmeier, S. Dresp, M. Gliech, Z. Jusys, P. Chernev, R. Kraehnert, H. Dau, P. Strasser, *J. Am. Chem. Soc.* **2017**, *139*, 2070 – 2082.

Manuscript received: November 11, 2020
Revised manuscript received: December 2, 2020
Version of record online: February 18, 2021

